BULLETIN OF THE POLISH ACADEMY OF SCIENCES
TECHNICAL SCIENCES, Vol. 58, No. 2, 2010
DOI: 10.2478/v10175-010-0021-7

Modelling of the microstructure and properties in the length scales varying from nano- to macroscopic

K.J. KURZYDLOWSKI*

Faculty of Materials Science and Engineering, Warsaw University of Technology, 141 Woloska St., 02-507 Warsaw, Poland

Abstract. The aim of this paper is to show the recent progress in multi length scale modelling of the engineering materials. This progress is demonstrated using a series of examples addressing, in particular, the role of effect of the grain boundaries in shaping properties of nano-polycrystalline metals.

Key words: multi length scale modelling, grain boundaries, nanomaterials.

1. Introduction

Modern engineering materials feature considerable complexity of their chemistry and structure. For example, chemical compositions of super-alloys are controlled at the level of ppm(s) with regard to a long list of elements. Also, new compositions are developed for a number of applications based on complex systems with a large number of phases, including intermetallic ones. Recently, structures of these complex chemistry alloys have been controlled at the level of nano-metres, with a focus on the fine grains, particles and interfaces. As a result, development of new engineering materials is challenging and can be efficiently carried out only with the use of tools for predicting at least some of the properties as a function of their chemistry and structure. The aim of this paper is to demonstrate, that such tools are currently available based on the numerical methods.

The capacity of the modern methods of predicting/modelling properties of engineering materials should be validated by examples, which include ab-initio modelling of the elastic properties of Al-Mg-La alloys, properties of point defects in Germanium and properties of the grain boundaries in Al alloys. Another example describes simulation of the grain growth in nano-polycrystalline metals via molecular dynamics and Monte Carlo method. Finally, the application of the Finite Element Method is described for predicting properties of nano-polycrystalline metals.

The examples used in this paper have been based on the original results obtained in [1–5] at the Materials Design Group at the Materials Science and Engineering Department of Warsaw University of Technology. More details on the methods used in this works can also be found in the following papers [6–10].

*e-mail: kjk@inmat.pw.edu.pl

2. Ab-initio modelling of structure and properties

Ab-initio computations are nowadays efficiently used to predict the crystal structure of metals and intermetallic compounds. They also allow for modelling the properties of point and planar defects. In the present paper, the advantages of ab-initio modelling is demonstrated using the following examples: (a) studies of elastic properties of La modified Al-Mg compounds developed for automotive applications, (b) predicting phase diagrams of W-Ta/V alloys for application in fusion reactors, (c) modelling phase transformations in FePt intermetallic alloys and (d) modelling point defects in Ge and finally (e) optimizing properties of the grain boundaries in an aluminium alloy.

2.1. Studies of elastic properties of La modified Al-Mg compounds. The La-X (X=Al,Mg) intermetallic compounds are used either as precipitates in certain magnesium alloys or by themselves in the context of hydrogen production and/or storage. However, optimized applications of these compounds require better understanding of their properties, which can be efficiently, at low cost, explored via comprehensive first principles computations, as shown by Wrobel et al. [10]. In this study, all independent components of the elasticity tensor, C_{ij}, and vibrational spectra of LaAl, $LaAl_2$, $LaAl_3$, $LaAl_4$, La_3Al_{11}, La_3Al, $La_{16}Al_{13}$, LaMg, $LaMg_2$, $LaMg_3$, La_2Mg_{17} and La_5Mg_{41} were computed. The polycrystalline bulk (B), shear (G), and Young's (E) moduli were also determined based upon the Hill criterion.

The results of computations are shown in Figs. 1–4, which illustrate the anisotropy of elastic properties of the intermetallic compounds in question. The computed values of the elastic constants are also collated in Tables 1 and 2.

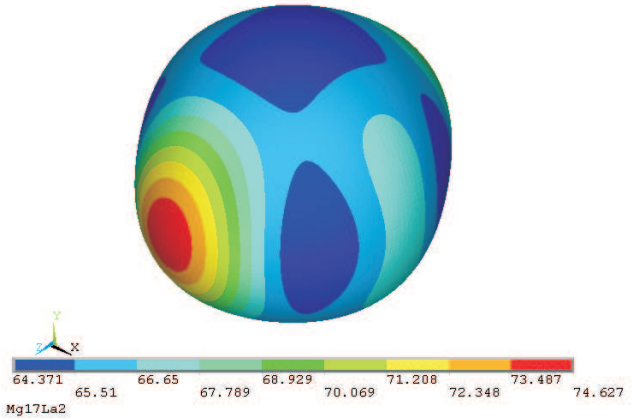

Fig. 1. The Young's modulus surface for the La_2Mg_{17} compound. The modulus is the largest in the <001> direction. La_2Mg_{17} is the most isotropic from all considered compounds

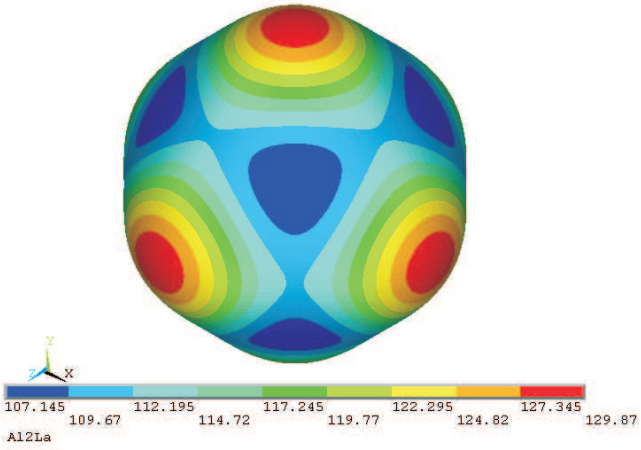

Fig. 3. The Young's modulus surface for the $LaAl_2$ compound. The modulus is the largest in the <100> and the smallest in the <111> direction. The anisotropy of the modulus is quite insignificant

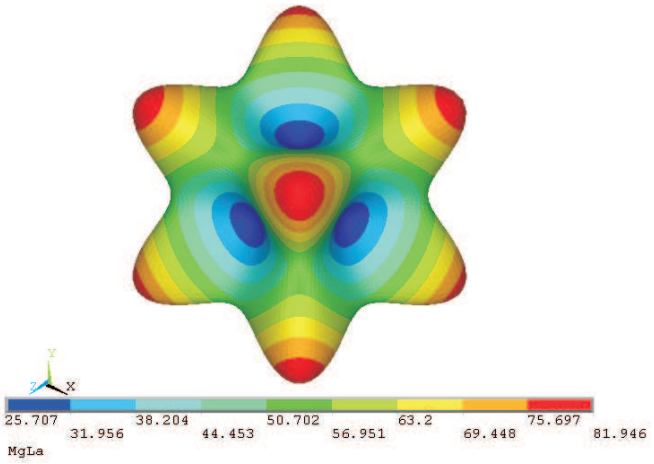

Fig. 2. The Young's modulus surface for the LaMg compound. It is the most anisotropic compound from all considered compounds. The Young's modulus in the <111> direction is more than three times larger than the modulus in the <100> direction

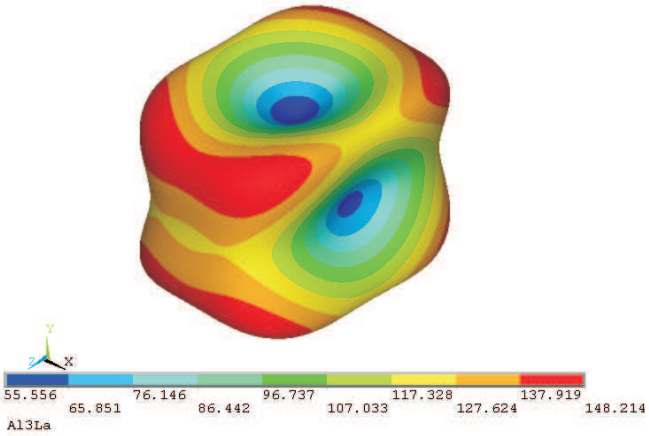

Fig. 4. The Young's modulus surface for the $LaAl_3$ compound. The Young's modulus in the <111> direction is almost three times larger than the modulus in the <010> direction

Table 1
Components of the elasticity tensor, C_{ij}, polycrystalline bulk (B), shear (G), and Young's (E) moduli from the Hill criterion for the La-Mg compounds. All are moduli are in GPa

La-Mg Structure	C_{11}	C_{12}	C_{13}	C_{33}	C_{44}	C_{66}	B	G	E
LaMg (Pm-2m)	47.4	28.7	–	–	36.9	–	34.9	21.4	52.9
$LaMg_2$ (Fd-3m)	57.9	25.0	–	–	22.2	–	36.0	19.7	49.9
$LaMg_3$ (Fm-3m)	39.3	26.5	–	–	36.6	–	37.4	26.5	64.3
La_2Mg_{17} (P63/mmc)	74.8	21.8	16.1	82.1	26.8	–	37.8	27.8	66.9
La_5Mg_{41} (I4/m)	70.9	17.0	17.1	74.8	30.5	17.8	35.4	26.2	62.9

Table 2
Components of the elasticity tensor, C_{ij}, polycrystalline bulk (B), shear (G), and Young's (E) moduli from the Hill criterion for the La-Al compounds. All are moduli are in GPa

La-Al Structure	C_{11}	C_{12}	C_{13}	C_{22}	C_{23}	C_{33}	C_{44}	C_{55}	C_{66}	B	G	E
LaAl (Cmem)	112.8	33.5	27.2	114.9	23.4	90.1	37.8	28.2	31.2	53.5	34.7	85.5
$LaAl_2$ (Fd-3m)	140.8	30.6	–	–	–	–	43.2	–	–	67.3	47.6	115.6
$LaAl_3$ (P63/mmc)	91.2	51.2	34.8	–	–	156.2	63.0	–	–	63.6	38.4	95.7
$LaAl_4$ (I4/mmm)	91.1	54.4	57.0	–	–	111.7	34.6	–	46.0	69.7	29.8	78.3
$LaAl_4$ (Imm2)	95.3	50.6	51.4	93.1	60.8	112.5	37.0	30.6	43.8	69.2	30.3	79.3
La_3Al_{11} (Immm)	127.6	43.7	44.9	117.8	46.1	114.5	56.6	63.0	55.2	69.9	48.8	118.6
La_3Al (Pm-3m)	56.7	31.0	–	–	–	–	22.8	–	–	39.6	18.1	47.1
La_3Al (P63/mmc)	59.3	30.3	23.8	–	–	–	24.2	–	–	38.2	19.4	49.8
La_3Al (Cm)	70.9	23.8	59.7	28.8	60.1	14.4	23.5	23.8	38.4	19.5	49.9	
$La_{16}Al_{13}$ P-62m	85.1	33.6	26.5	–	–	78.2	27.4	–	–	46.7	26.9	67.6

It has been found that La_3Al_{11}compound has the highest bulk modulus followed by the two $LaAl_4$ compounds. The polycrystalline moduli for the two La_3Al compounds are nearly identical, but the same is not the case for their computed C_{ij}. The shear elastic constants for La_3Al (C_{44}) and La_3Al_{11} (C_{44}, C_{55}, C_{66}) are highest which suggests that bonding is more directional in these materials than in the other compounds.

It can be also noted (for details see [10]) that the shear elastic constants for La_3Al_{11}, C_{55} exceed both C_{44} and C_{66}, so that resistance to shear is greatest in the a–c plane. The magnitudes of the longitudinal elastic constants, C_{11}, C_{22}, and C_{33} are an indication of the extent to which the compound resists elastic deformation along the a-, b-, and c-axes, respectively. Shiltz and Smith [11] measured the single crystal C_{ij} of $LaAl_2$ over a temperature range of 4.2 – 300 K using a pulse-echo-overlap technique. At 4.2 K, they reported $C_{11} = 148.2$, $C_{12} = 31.9$ and $C_{44} = 43.6$ GPa. These computed C_{ij} for $LaAl_2$ at 0 K ($C_{11} = 140.8$, $C_{12} = 30.6$, $C_{44} = 43.2$ GPa) are in reasonably close accord with these experimentally-measured values. This positive validation of the results of computations implies that they can be used to optimize chemical composition of the La-Mg/Al light alloys for particular applications, either via particle strengthening or directly in single-phase form.

2.2. Predicting phase diagrams of W-Ta/V alloys for application in fusion reactors. Fusion reactors are exposed to harsh in-service conditions which require the use of radiation resistance materials. Tungsten is one of the most radiation resistant materials, which, however, exhibits considerable brittleness in at low and elevated temperatures. In order to improve mechanical properties of tungsten, various alloying strategies are currently explored, with Tantalum and Vanadium being one of the alloying elements. The available experimental phase diagrams for W-Ta/V alloys describe the high temperature limit close to the melting point. These diagrams exhibit only the solid solution phases and show no ordered intermetallic phases that in principle should be expected to form at low temperatures.

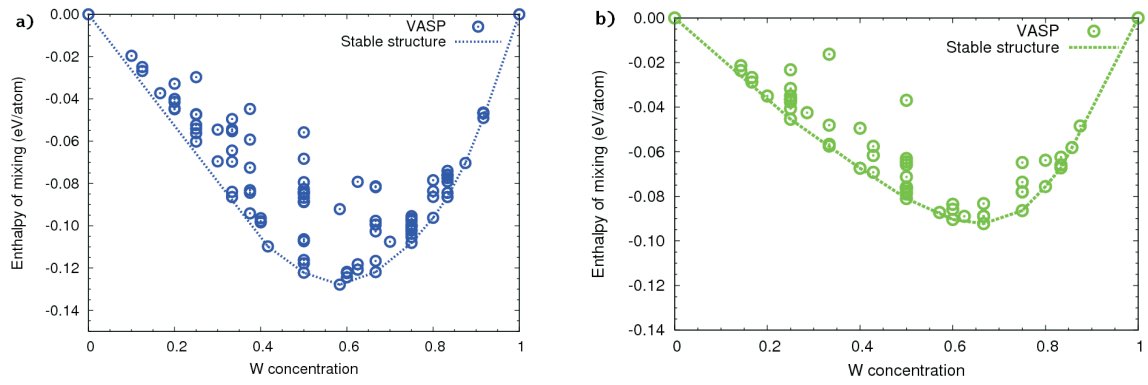

Fig. 5. Calculated enthalpy of mixing for a) W-Ta and b) W-V alloys. The most stable structure are connected by the line

Experimental investigations of the W-V/Ta phase diagram are technically challenging, among others because of the high melting temperatures of these elements, and time consuming. In this situation, ab-initio calculations have been carried [12–14] to compare enthalpies of mixing for large sets (∼150 structures) of alloy configurations, considering several alternative ordered structures corresponding to the same chemical composition. In this way, the lowest energy intermetallic compounds were identified that are expected to dominate alloy microstructures, and hence the low temperature part of phase diagrams, for both alloys, results of which are presented in Fig. 5. These results provide estimates of enthalpy of formation for W-Ta/V alloys as a function of concentration of alloying elements. Such estimates can be subsequently used to predict the most stable phases.

2.3. Modelling phase transformations in FePt intermetallic alloys. Thin films of the FePt compound are known to exhibit a high magnetic anisotropy which makes them attractive in data storage applications. Fe and Pt atoms form in general three superstructures, which are shown in Fig. 6. The most suitable for applications is superstructure denoted as "c", which, unfortunately, is not energetically stable if fabricated in form of thin films due to surface relaxation, which results in formation of domains with "a" and "b" superstructures, which arrange themselves in an anti-phase manner. In order to obtain an insight into the kinetics of phase transformations in FePt alloys, Kinetic Monte Carlo calculations have been carried out [15], which provided estimates of average domain size and surface fractions of domains with different superstructure as a function of time – see Figs. 7 and 8 and for different temperatures. Such estimates can be used to optimize heat treatment of FePt thin films for applications in storage devices.

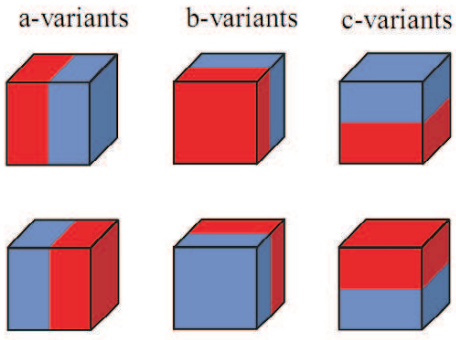

Fig. 6. Mesoscale voxels showing 6 $L1_0$ orientations (variants a+, a-, b+, b-, c+ and c-)

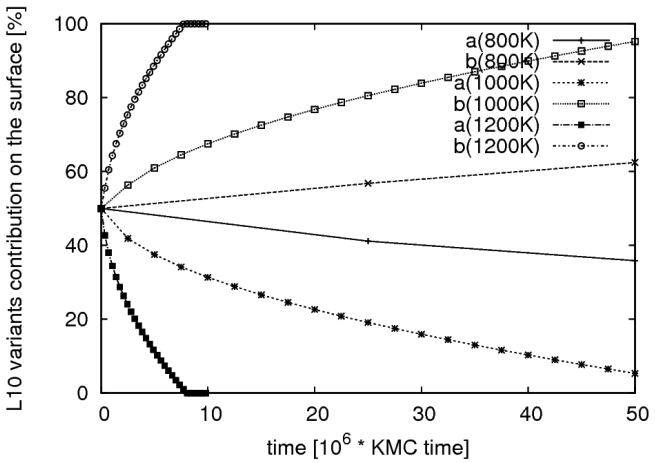

Fig. 7. Fraction of the a- and b-variant $L1_0$ domains in the surface layer in relation of time for different temperatures of the simulation: 800 K, 1000 K and 1200 K

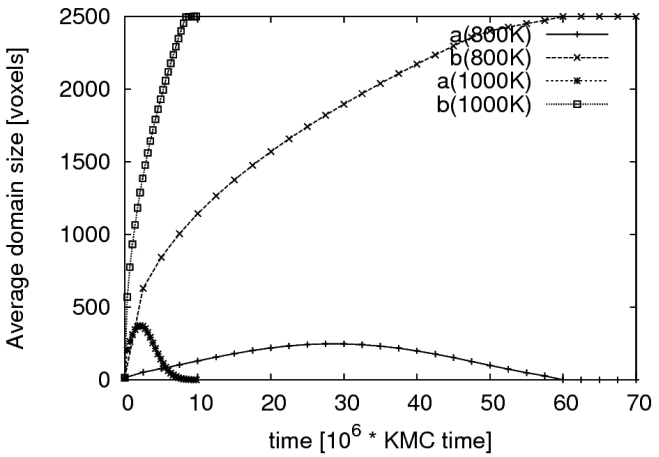

Fig. 8. Average volume of the $L1_0$ domains in relation of time for different temperatures of the simulation: 1000 K and 1200 K

The projection of the FePt surface in the different MC time steps of the simulation is presented in Fig. 9. The results shown in this figure can be used to distinguish specific stages in the transformations into a- or b- variants, taking place in the thin layers of FePt. They can be also used to examine the mechanism of this transformation, which is controlled by the growth of the bigger domains at the expense of the smaller ones. The domain growth is more rapid in the early stages of the process due to the higher number of small domains. The relaxation becomes much slower when there are only few large domains (Fig. 9).

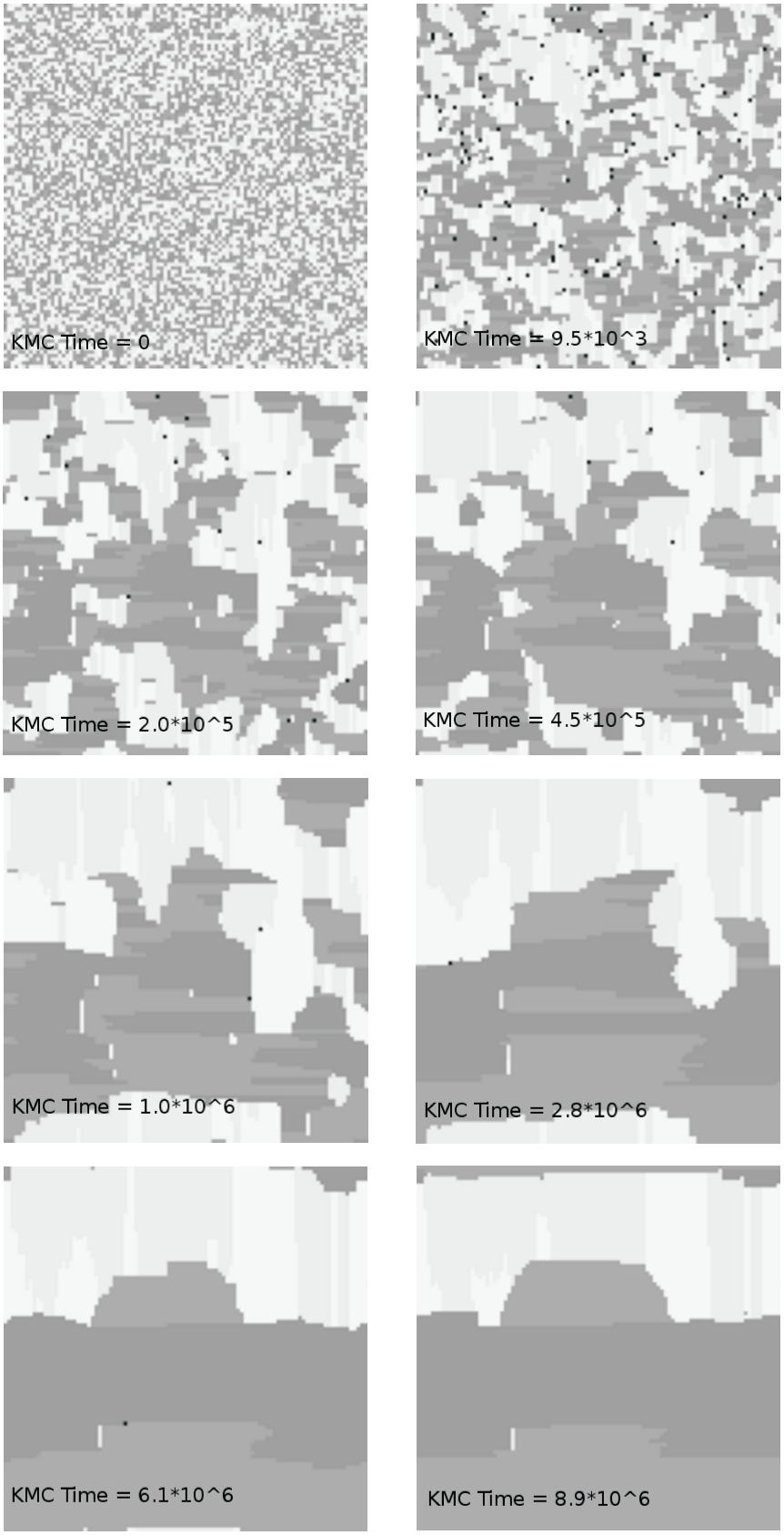

Fig. 9. Images presenting temporal domains evolution. Different colours indicate voxels with particular $L1_0$ superstructure orientations: variants a+, a- are light gray, b+ and b- are dark gray. Black points are the fields with c-variant orientation

2.4. Modelling the grown-in defects in Ge. Germanium single crystals have already been used in electronic industry in such applications as solar cells for space applications, terrestrial concentrator photovoltaic arrays (CPV) and light emitting diodes (LED). Recently, applications of germanium in complementary metal-oxide semiconductors (CMOS) have attracted considerable attention [16]. Its high carrier mobility and low-voltage operation make Ge a possible alternative to Si as active layer in advanced electronics devices [17]. However, technology of growing such single crystals is far from being fully mastered, among others, due to insufficient understanding of the properties of grown-in defects formed during the crystal growth process [18]. These defects have been recently investigated via multi-scale modelling approach based on ab initio calculations in atomic scale (for more information see [3]). The results obtained within these studies were used to predict the density and size of vacancies clusters in Ge crystals grown under varied technological regimes, as exemplified in Fig. 10.

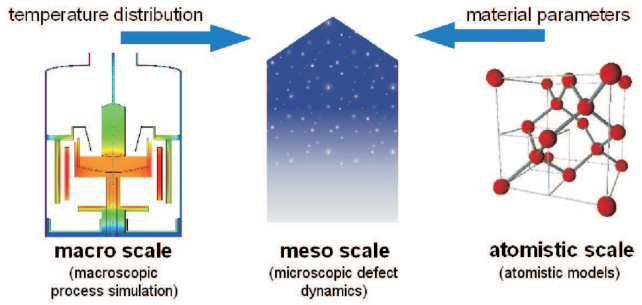

Fig. 10. Schematic explanation of a multi-scale model of defect dynamics during crystal growth after Ref. 3

2.5. Optimizing properties of the grain boundaries in aluminium alloys. More recently ab-initio techniques have been used to model the properties of grain boundaries in metals (e.g. [19]). An example of the results obtainable with ab-initio methods is given in Fig. 11, which illustrate changes in the energy of flat grain boundaries in Al as a function of the rotation angle. It should be noted, however, that the ab-initio computations are currently limited to a relatively low number of atoms, on average less than 500. This imposes a significant limitation on the geometry of the grain boundaries and the angle of rotation between the crystal lattices of the grains. As ab-initio calculations are carried out under the assumption of periodic boundary conditions, so called general grain boundaries, with "random" rotation angles of the crystal lattice cannot, as yet, be modelled. Nevertheless, the currently available models do provide a useful insight into the properties of so called special grain boundaries, with specific rotations angles, which comprise a significant fraction of the grain boundaries in ultra-fine- and nano-grained aluminium alloys (see for example [20, 21]). Additionally, some processes taking place at the special grain boundaries are also observed for their random counterparts, usually with different kinetics or dynamics (see for example [22]).

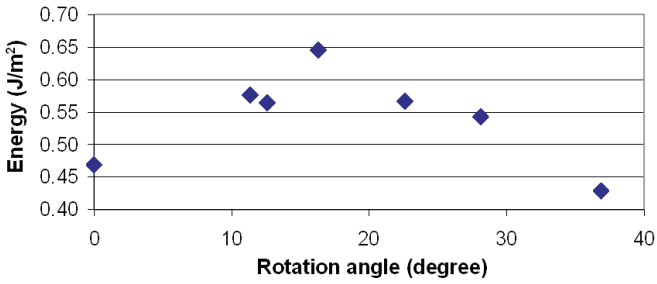

Fig. 11. The energy of flat grain boundaries plotted against the rotation angle between two neighbouring crystals

2.6. Application of ab-initio methods. In order to illustrate applications of ab-initio, the following text describes how modelling of the grain boundaries in Al can be used to optimize corrosion resistance of 2014 aluminium alloy. Figure 12 shows a system of grain boundaries revealed in a sample of such an alloy after exposure to the environment causing grain boundary corrosion. It can be noted from the micrographs presented in this figure that grain boundaries of different mis-orientation show different resistance to inter-granular corrosion – see also Fig. 13.

Generally, the difference in the corrosion resistance of different types of grain boundaries can be related to the differences in their energies. On the other hand, the energy of the grain boundaries, and in turn their corrosion resistance, is also influenced by grain boundary segregation effects, as demonstrated by recent studies using the ab-initio method [23]. The ab-initio results describing the tendency for the segregation of alloying elements at grain boundaries of different orientation angle in aluminium are given Table 3.

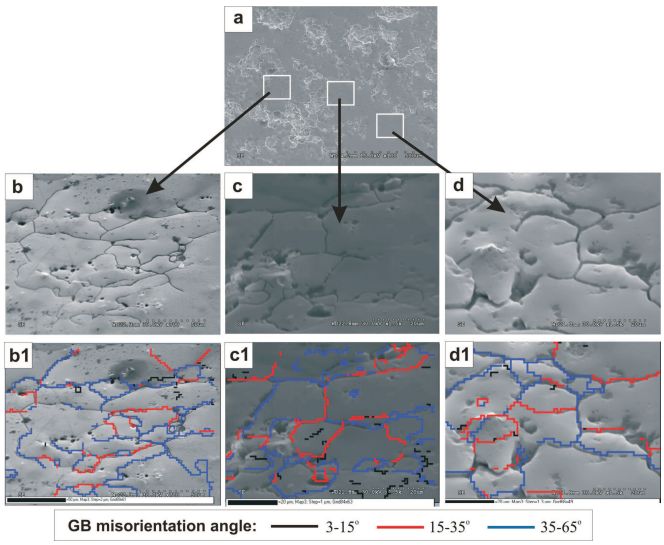

Fig. 12. Grain boundaries revealed in 2014 aluminium alloys: the coloured lines indicate the grain boundaries of mis-orientation angle from different ranges

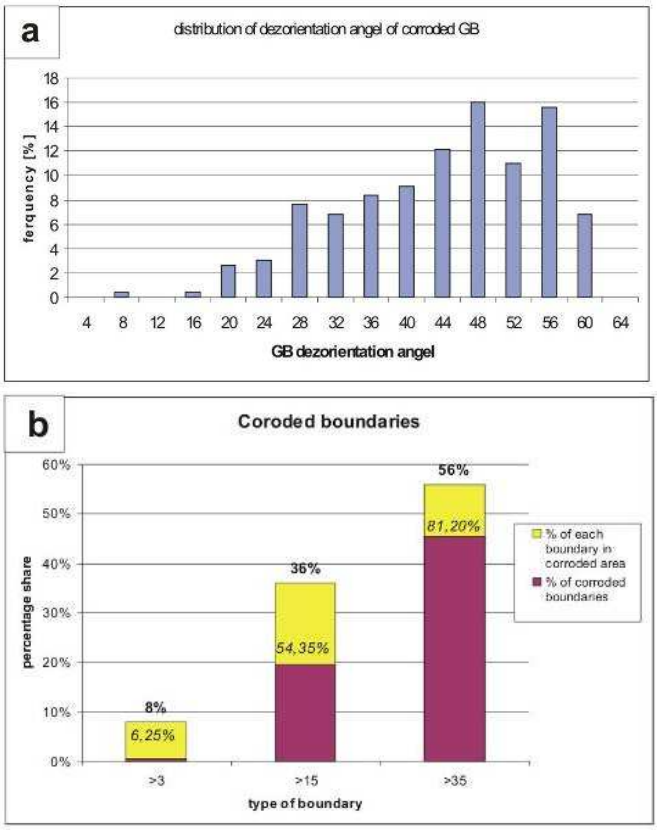

Fig. 13. Distribution function of the grain boundaries mis-orientation angle (a) and propensity of grain boundaries to grain boundary corrosion

Table 3
Changes in the grain boundary energy, in J/m^2, due to alloying additions at the grain boundaries in aluminium

Angle	Clean	Cu	Fe	Mg	Mn
12.55	-0.4053	0.01596	1.21075E-05	-4.17884E-06	1.23441E-05
22.62	-0.4053	-0.00351	1.20575E-05	-3.97486E-06	1.33038E-05
36.87	-1.0602	-0.00017	1.81741E-05	-6.28934E-06	-1.79448E-05

These results have been obtained for twist boundaries. It can be noted that for all 3 grain boundaries analyzed, there is a strong tendency for Mg segregation. By contrast, iron does not segregate at all and Mn and Cu segregate only to the boundaries with a higher orientation angle. The results also clearly illustrate the segregation effect on the energy of the grain boundaries and in turn on the corrosion resistance.

3. A molecular dynamic and Monte Carlo simulations of grain growth

Molecular dynamics is widely used in the modelling of engineering materials when a larger number of atoms need to be considered. An example of such a situation is the modelling of processes taking place at grain boundaries, in particular grain shrinking/growth under the action of grain boundary surface tension [24]. A model geometry used to simulate changes in small grains, typical of nano-polycrystalline metals, is shown in Fig. 14.

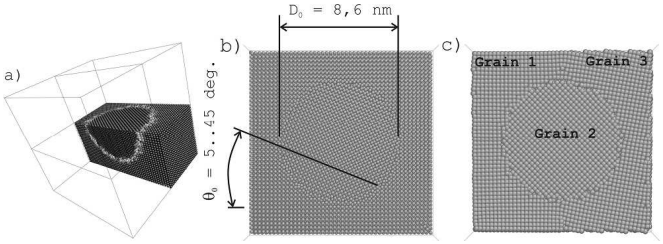

Fig. 14. A special case of non-flat grain boundaries: (a) general view of the modelled volume; (b) 2-D image of a small grain embedded into a larger one; (c) the case of three grains– for details see Ref. 20

Such model geometry has been used to predict the kinetics of grain disappearance, which in turn directly determines the rate of grain growth in fine, nano-grained polycrystalline aggregates.

Monte Carlo modelling can be used to model processes at the scale of microns, such as grain growth. The computing power available in a standard laboratory nowadays allows for the modelling of grain growth with a higher level of sophistication than in the past. The currently available models of grain growth take into account the true geometry of the grain boundaries and the diversity in their properties, as illustrated in Fig. 15.

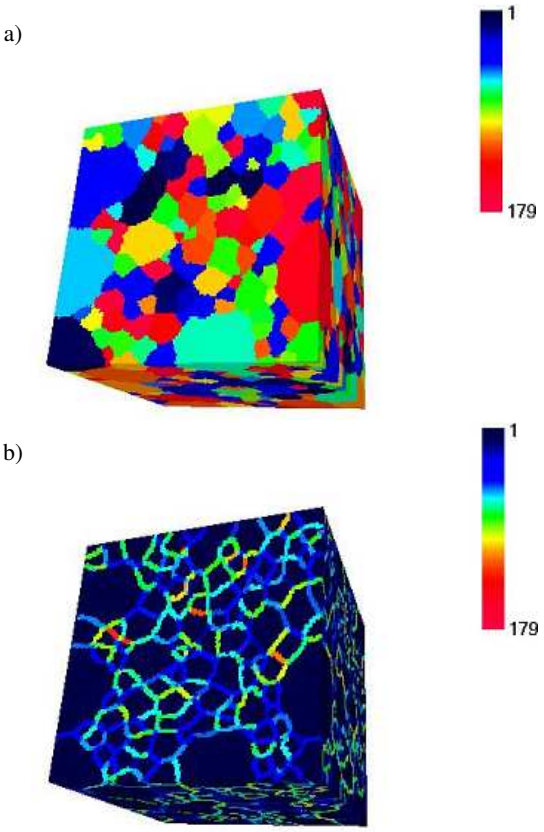

Fig. 15. A model of the grain boundary geometry and their properties adopted in Ref. 25 – (a) Map of grain orientations and (b) grain rotation angles of boundaries for a structure with non-homogeneous grain size distribution

A model developed by Wejrzanowski [25] has been used to study the effect of special grain boundaries on the kinetics of grain growth. The results, shown in Fig. 16, for two polycrystalline structures, are characterized by a large fraction of the special grain boundaries (denoted as "textured", as such boundaries are more likely in materials exhibiting crystallographic texture).

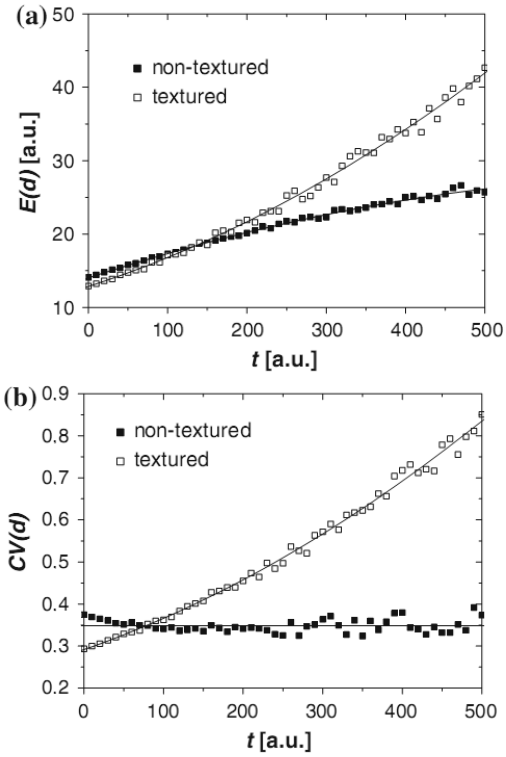

Fig. 16. The results of modelling of grain growth in polycrystalline materials containing different fractions of special grain boundaries-changes as a function of time: (a) in the mean size of grains, E(d); (b) in the diversity of the grain size, defined in terms of the coefficient of variation, CV(d)

The results clearly show that a high fraction of special grain boundaries brings about a higher rate of grain growth (Fig. 16a). It also brings about a tendency for abnormal grain growth, as indicated by the results shown in Fig. 16b.

4. Finite Element Models of plasticity of nano-metals

It has long been recognized that grain boundaries influence the properties of a wide range of metallic materials, particularly in the case of fined and nano-grained polycrystalline metals. The effect of grain boundaries on the mechanical properties of metals is especially strong at temperatures below approximately 0.3 T_m (T_m – the melting temperature). The strengthening effect of the grain size on the yield stress was described by Hall [26], Petch [27] and on the flow stress by Armstrong and co-workers [28]. There have been also numerous papers published over the last 30 years (for example [29–36]) on the influence of the grain boundaries on the plastic flow of polycrystalline materials with the grain size in the range of micrometres.

The plastic deformation of nano-polycrystalline metals differ significantly from the deformation of their micrometre counterparts by the fact that in the latter case grain boundaries must be considered as 3-D elements. This is due to the fact, that in nano-sized polycrystals the atoms residing at the grain boundaries account for a considerable fraction of the material's volume. With this in mind, a finite element model of nano-polycrystalline aluminium alloy has been developed, which is illustrated in Fig. 17 (for more details see [4, 32]).

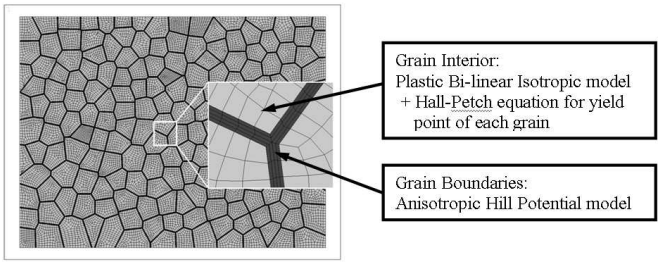

Fig. 17. Finite element model of nano-polycrystalline aluminium developed in Ref. 36

The model shown in Fig. 18 has been used to study the effect of the variation of the properties of the grain boundaries on the macroscopic flow stress. In particular, the effect of grain boundary sliding has been also investigated – results are shown in Fig. 19, which illustrates the relative accommodation of the macroscopic strain at the grain boundaries and in the grain interiors. It can be noted that the grain boundaries, and particularly some triple points, absorb relatively large deformation at the early stages of the plastic straining. This preferential deformation at the grain boundaries results in the grain boundary softening (inverse Hall-Petch relationship) and necking of nano-polycrystalline metals.

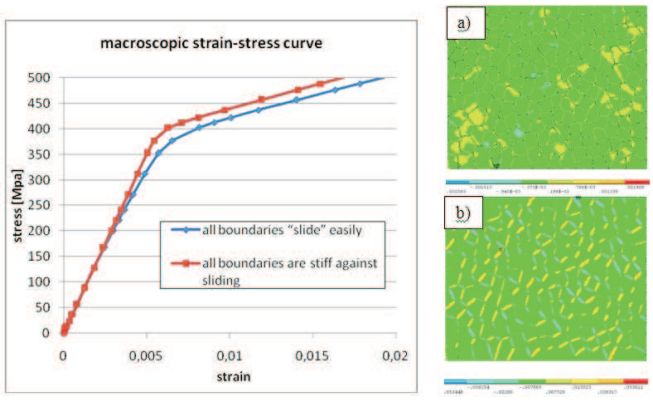

Fig. 18. Results of modelling of the grain boundary sliding in a nanocrystalline material: a) all boundaries are stiff against sliding, b) all "slide" easily

The inverse Hall-Petch relationship as en effect of influence of the grain boundaries volume fraction is shown in Fig. 19. The growth of influence of grain boundaries on the flow stress for metals in nanometric regime rapidly in-

crease with changing the volume fraction of atoms residing at the grain boundaries [37].The softening of polycrystalline nanometals, for the grain size les then approximately 20nm, due to strain absorption in grain boundaries has a larger impact than mechanisms of grains stiffening which are responsible for standard H-P relation.

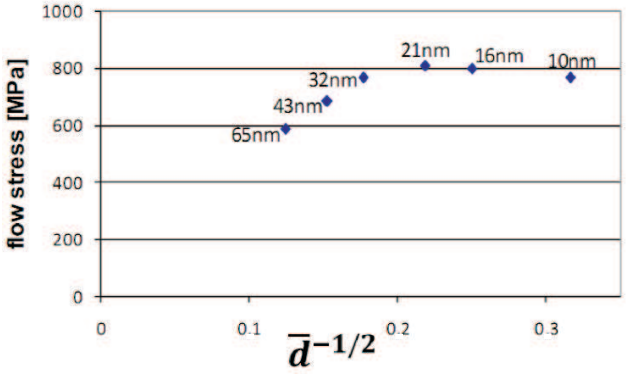

Fig. 19. The inverse Hall-Petch relationship as an influence of the grain boundaries volume fraction

5. Concluding comments

The results presented here have been collated with the intention to demonstrate that the currently available modelling methods allow for optimizing the structure/properties of polycrystalline materials.

The examples provided in this paper to validate this statement include modelling: (a) – at the atomistic level (ab-initio); (b) – at the level of micrometres (molecular dynamic) and (c) – at meso- and macroscopic level. At each of the above indicated scales, modelling provides a better insight into grain boundary processes and into the influence of these processes on the properties of polycrystalline materials.

In conclusion, it has been shown that there are tools available, which can be used to optimize the properties of polycrystalline materials by engineering the structure/properties of the grain boundaries.

Acknowledgements. A part of this work was carried out within a NANOMET Project financed under the European Funds for Regional Development (Contract No. POIG.01.03.01-00-015/08).

REFERENCES

[1] R. Sot, "Properties of crystal networks of the chosen aluminides determined ab initio", *PhD Thesis*, Warsaw University of Technology, Warsaw, 2006, (in Polish).

[2] T. Wejrzanowski, "Modelling of the influence of grain size heterogenity on their growth in the monophase polycrystal materials", *PhD Thesis*, Warsaw University of Technology, Warsaw, 2006 (in Polish).

[3] P. Spiewak, "Modelling of properties of point defects and their clusters in dislocation – free single crystal germanium", *PhD Thesis*, Warsaw University of Technology, Warsaw, 2009.

[4] R. Dobosz, "Influence of grain boundaries on plastic resistivity of polycrystal nanomaterials", *PhD Thesis*, Warsaw University of Technology, Warsaw, 2010, (in Polish).

[5] M. Muzyk, "Modelling of grain boundary structure and properties in aluminium and its alloys", *PhD Thesis*, Warsaw University of Technology, to be published, (in Polish).

[6] R. Sot and K.J. Kurzydlowski, "Atomic modelling of point defects in B2-RuAl", *Materials Science – Poland* 23, 407–411 (2005).

[7] M. Muzyk and K.J. Kurzydlowski, "Density functional theory calculations of properties of point defects in B2-NiAl intermetallic compound", *Scripta Materialia* 62, (2010), to be published.

[8] R. Sot and J. Piechota, "First principles study of Al(100) twisted interfaces", *Solid State Phenomena* 129, 131 (2007).

[9] W.L. Spychalski, K.J. Kurzydłowski, and B. Ralph, "Computer study of inter- and intra-granular surface crack in brittle polycrystal", *Materials Characterization* 49, 45–53 (2002).

[10] J. Wróbel, L.G. Hector, T. Wejrzanowski, and K.J. Kurzydłowski, "Mechanical and thermodynamical properties of X-La intermetallic compounds on the basis of computations from first principles (X=Al,Mg)", *Material Engineering School* 1, CD ROM (2009), (in Polish).

[11] R. J. Schlitz and J. F. Smith, "Elastic constants of some MAl_2 single crystals", *J. Appl. Phys.* 45, 4681 (1974).

[12] V. Blum and A. Zunger, "Prediction of ordered structures in the bcc binary systems of Mo, Nb, Ta, and W from first-principles search of approximatelly 3,000,000 possible configurations", *Phys. Rev.* B 72, 020104 (2005).

[13] S.V. Barabash, R.V. Chepulskii, V. Blum, and A. Zunger, "First-principles determination of low-temperature order and ground states of Fe-Ni, Fe-Pd, and Fe-Pt", *Phys. Rev.* B 80, 220201 (2009).

[14] G. Kresse and J. Furthmüller, "Efficient iterative schemes for ab initio total-energy calculations using a plane-wave basis set", *Phys. Rev.* B 54, 11169 (1996).

[15] R. Kozubski, M. Kozłowski, J. Wróbel, T. Wejrzanowski, K. Kurzdłowski, Ch. Goyhenex, M. Rennhofer, and S. Malinov, "Atomic ordering in nano-layered FePt: multiscale Monte Carlo simulation", *Computational Materials Science* 48, (2010), to be published.

[16] M.L. Lee, E.A. Fitzgerald, M.T. Bulsara, M.T. Currie, and A. Lochtefeld, "Strained Si, SiGe, and Ge channels for high-mobility Metal-Oxide-Semiconductor Field-Effect Transistors", *J. Appl. Physics* 97, 011101 (2005).

[17] *The International Technology Roadmap for Semiconductors*, http://www.itrs.net (2009).

[18] J. Vanhellemont, O. De Gryse, S. Hens, P. Vanmeerbeek, D. Poelman, P. Clauws, E. Simoen, C. Claeys, I. Romandic, A. Theuwis, G. Raskin, H. Vercammen, and P. Mijlemans, "Grown-in lattice defects and diffusion in Czochralski-grown germanium", *Defect and Diffusion Forum* 230–232, 149–176 (2004).

[19] E. Wachowicz and A. Kiejna, "Effect of impurities on grain boundary cohesion in bcc iron", *Computational Materials Science* 43, 736–743 (2008).

[20] M. Winning, G. Gottstein, and L.S. Shvindlerman, "Stress induced grain boundary motion", *Acta Materialia* 49, 211–219 (2001).

[21] P. Lejcek, S. Hofmann, and V. Paidar, "Solute segregation and classification of [100] tilt grain boundaries in α-iron: conse-

quences for grain boundary engineering", *Acta Materialia* 51, 3951–3963 (2003).

[22] C. Zheng and Y.W. Zhang, "Atomistic simulations of mechanical deformation of high-angle and low-angle nanocrystalline copper at room temperature", *Materials Science & Engineering* A 423, 97–101 (2006).

[23] A. Balkowiec, J. Brunner, J. Michalski, H. Matysiak, and K.J. Kurzydlowski, "Grain boundary mis-orientation effect on intergranular corrosion in aluminium sheets", 11^{th} *Int. Conf. on Aluminium Alloys* 1, CD-ROM (2008).

[24] T. Wejrzanowski, M. Spychalski, R. Pielaszek, and K.J. Kurzydlowski, "Grain boundary migration in nanocrystalline iron", *Solid State Phenomena* 129, 145–150 (2007).

[25] T. Wejrzanowski and K.J. Kurzydlowski, "Modelling of grain growth in nano-polycrystalline materials", *5th Int. Conf. on Mechanics & Materials in Design* 1, CD-ROM (2006).

[26] E.O. Hall, "The deformation and ageing of mild steel: II Characteristics of the Lüders deformation", *Proc. Phys. Soc.* B 64, 742–748 (1951).

[27] N.J. Petch, "The cleavage stress of polycrystals", *J. Iron. Steel Inst.* 174, 25–28 (1953).

[28] R.W. Armstrong, "The influence of polycrystal grain size on mechanical properties", *Advances in Materials Research* 4, 101–146 (1970).

[29] S. Berbenni, V. Favier, and M. Berveiller, "Micro–macro modelling of the effects of the grain size distribution on the plastic flow stress of heterogeneous materials", *Computational Materials Science* 39, 96–105 (2007).

[30] H.C. Choi and K.T. Park, "The effect of carbon content on the Hall-Petch parameter in the cold drawn hypereutectoid steels", *Scripta Materialia* 34, 857–862 (1996).

[31] C. Mercer and W.O. Soboyejo, "Hall-Petch relationships in gamma titanium aluminides", *Scripta Materialia* 35, 17–22 (1996).

[32] R. Mahmudi, "Grain boundary strengthening in a fine grained aluminium alloy", *Scripta Metallurgica et Materialia* 32, 781–786 (1995).

[33] N. Hansen, "Boundary strengthening in undeformed and deformed polycrystals", *Materials Science & Engineering* A 409, 39–45 (2005).

[34] I. Watanabe, K. Terada, E.A. de Souza Neto, and D. Peric, "Characterization of macroscopic tensile strength of polycrystalline metals with two-scale finite element analysis", *J. Mechanics and Physics of Solids* 56, 1105–1125 (2008).

[35] D.S. Balint, V.S. Deshpande, A. Needleman, and E. Van der Giessen, "Discrete dislocation plasticity analysis of the grain size dependence of the flow strength of polycrystals", *Int. J. Plasticity* 24, 2149–2172 (2008).

[36] R. Dobosz, T. Wejrzanowski, and K.J. Kurzydlowski, "Modelling the influence of the structure on the properties of nanometals", *Computer Methods in Materials Science* 9, 1 (2009).

[37] S.C. Tjong and H. Chen, "Nanocrystalline materials and coatings", *Materials Science and Engineering* R 45, 1–88 (2004).